ACS APPLIED MATERIALS & INTERFACES

www.acsami.org

Research Article

Rapid and Large-Area Visualization of Grain Boundaries in MoS_2 on SiO_2 Using Vapor Hydrofluoric Acid

Xuge Fan,* Rita Siris, Oliver Hartwig, Georg S. Duesberg,* and Frank Niklaus*

Cite This: *ACS Appl. Mater. Interfaces* 2020, 12, 34049–34057

Read Online

ACCESS | Metrics & More | Article Recommendations | Supporting Information

ABSTRACT: Grain boundaries in two-dimensional (2D) material layers have an impact on their electrical, optoelectronic, and mechanical properties. Therefore, the availability of simple large-area characterization approaches that can directly visualize grains and grain boundaries in 2D materials such as molybdenum disulfide (MoS_2) is critical. Previous approaches for visualizing grains and grain boundaries in MoS_2 are typically based on atomic resolution microscopy or optical imaging techniques (i.e., Raman spectroscopy or photoluminescence), which are complex or limited to the characterization of small, micrometer-sized areas. Here, we show a simple approach for an efficient large-area visualization of the grain boundaries in continuous chemical vapor-deposited films and domains of MoS_2 that are grown on a silicon dioxide (SiO_2) substrate. In our approach, the MoS_2 layer on a SiO_2/Si substrate is exposed to vapor hydrofluoric acid (VHF), resulting in the differential etching of SiO_2 at the MoS_2 grain boundaries and SiO_2 underneath the MoS_2 grains as a result of VHF diffusing through the defects in the MoS_2 layer at the grain boundaries. The location of the grain boundaries can be seen by the resulting SiO_2 pattern using optical microscopy, scanning electron microscopy, or Raman spectroscopy. This method allows for a simple and rapid evaluation of grain sizes in 2D material films over large areas, thereby potentially facilitating the optimization of synthesis processes and advancing applications of 2D materials in science and technology.

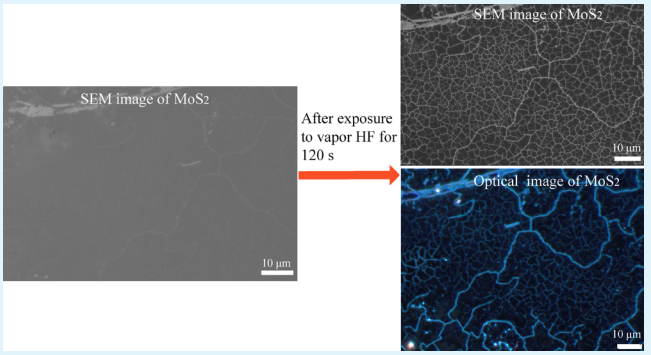

KEYWORDS: *2D materials, TMDS, MoS_2, grain boundaries, grains, vapor hydrofluoric acid, chemical vapor deposition*

1. INTRODUCTION

Two-dimensional (2D) materials such as molybdenum disulfide (MoS_2) have been studied for use in potential applications[1−3] such as transistors,[4] light emitters,[5] photodetectors,[6] modulators,[7] pressure sensors,[8] resonators,[9] biosensors,[10] gas sensing,[11] photocatalysis,[12] and electrochemical applications.[13] For using these 2D materials in device applications, it is critically important to realize the industrial-scale and reliable synthesis of high-quality monolayers of the 2D materials at low cost. Chemical vapor deposition (CVD) is a potential large-scale 2D material synthesis approach suitable for industrial applications and one of the most developed approaches for the preparation of large-area MoS_2 of good quality.[14−17] For the development and optimization of CVD-grown single-layer MoS_2, it is important to characterize the properties of the grown MoS_2 layers that typically consist of irregularly shaped individual grains that connect the adjacent grains[18−21] through grain boundaries. As a result, the grain sizes and grain boundaries of the domains or continuous films of MoS_2 have an important impact on its electrical,[18,22−24] optical,[18] optoelectronic,[25,26] mechanical,[27,28] and chemical properties[29] as well as on the characteristics of devices made of MoS_2. Furthermore, the properties of grain boundaries in MoS_2 might be beneficially used in specific applications by controlled defects engineering.[30−32] For the above reasons, fast and simple methods to directly observe the large-area distribution of grains and grain boundaries in MoS_2 are of increasing importance.

Grains and grain boundaries in MoS_2 films can be characterized by atomic resolution using transmittance electron microscopy (TEM)[18−20] and scanning tunneling microscopy (STM),[32,33] providing detailed information about the crystal structure of the grains and the grain boundaries. The MoS_2 grain boundaries can also be identified using atomic force microscopy (AFM) by decorating a self-assembled octadecylphosphonic acid monolayer on the MoS_2 surface.[34] However, these techniques are time-consuming, require complex sample preparation procedures, and/or are limited to the characterization of very small areas. Another approach to

Received: April 15, 2020
Accepted: July 3, 2020
Published: July 3, 2020

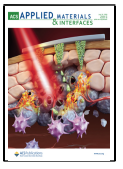

https://dx.doi.org/10.1021/acsami.0c06910
ACS Appl. Mater. Interfaces 2020, 12, 34049−34057

observe grain boundaries in MoS_2 is the use of nonlinear optics.[35−38] For instance, the grain boundaries between the adjacent MoS_2 grains can be distinguished by stacking MoS_2 bilayers and using photoluminescence imaging based on second harmonic generation.[37] However, photoluminescence imaging is generally limited to MoS_2 domains that feature a large rotation of the crystal axis as compared to the neighboring grains, requires sophisticated optical systems, and is typically slow.[39] Compared to photoluminescence imaging, a faster approach for visualizing grain boundaries in CVD-grown MoS_2 is multiphoton microscopy based on third-harmonic generation, which is also independent of the degree of crystal axis rotation.[39] Yet, this approach still requires a relatively sophisticated optical system and therefore is not easily accessible. Grain boundaries in CVD-grown MoS_2 layers can also be visualized by oxidizing MoS_2 using UV irradiation in a moisture-rich environment and subsequently imaging the layer with scanning electron microscopy (SEM) or AFM.[40] However, with this approach, additional visible oxidized line defects within the MoS_2 grains were produced alongside the grain boundaries because of easy oxidation of MoS_2.[40] The grains and grain boundaries of large MoS_2 layers were also visualized by depositing nematic liquid crystals on the MoS_2 layers in combination with polarized optical microscopy[41] or by visualizing the differential diffusion of gold on the surface of MoS_2 between the grain boundaries and the inner grain areas after depositing gold on the MoS_2 surface using optical microscopy.[42] However, these techniques require elaborate and controlled preparation of the MoS_2 samples.

Here, we present a simple and rapid method for visualizing grain boundaries in large areas of CVD-grown single-layer MoS_2 on a SiO_2 surface using SEM, optical microscopy, or Raman spectroscopy. Similar to the previously reported method for observing grain boundaries in CVD-grown graphene placed on a SiO_2 surface using vapor hydrofluoric acid (VHF) exposure,[43] in the proposed method, we first expose the MoS_2 layer on the SiO_2 surface to VHF, which causes VHF molecules to diffuse through the defects in the lattice structure of the MoS_2 grain boundaries. The diffusion of the VHF through these defects results in etching of SiO_2 underneath MoS_2, with a difference between the etching speed of SiO_2 directly at the grain boundaries and the etching speed of SiO_2 in the areas below the grains away from the grain boundaries. The resulting etch pattern in the SiO_2 layer along the MoS_2 grain boundaries is then visible and can be imaged using optical microscopy, SEM, or Raman spectroscopy. Because the MoS_2 and the underlying SiO_2 layers are exposed to VHF and etched to some extent in our method, this is an invasive approach. SiO_2 is one of the most commonly used growth substrates for large-area CVD-grown MoS_2, and thus, our method will be useful in the development, characterization, and optimization of large-area MoS_2 synthesis processes.

2. EXPERIMENTAL SECTION

In all experiments, we used CVD-grown single-layer MoS_2 on a SiO_2/Si substrate that was bought from 2D Semiconductors (USA), in which the SiO_2 layer was 285 nm thick. MoS_2 was composed of domains with continuous films and individual grains with visible grain boundaries that were not fully stitched to the adjacent MoS_2 grains. For VHF etching, we exposed the SiO_2/Si chips with the MoS_2 films to VHF that was evaporated from a liquid HF solution with a HF concentration of 25%. The VHF reacts with SiO_2 underlying the grain boundaries of the MoS_2 layer by penetrating the defects of the grain boundaries. To control the amount of H_2O that is present at the substrate surfaces, the substrate temperature was kept at 40 °C.[44,45] For details on the experimental setup of the VHF chamber, our previous publication on the visualization of grain boundaries in graphene could be referred.[43] The VHF etching of SiO_2 involves reactions 1 and 2.

$$SiO_2 + 2H_2O \rightarrow Si(OH)_4 \quad (1)$$

$$Si(OH)_4 + 4HF \rightarrow SiF_4 \uparrow + 4H_2O \quad (2)$$

Before and after exposing MoS_2 on the SiO_2/Si substrate to VHF for different times, we used optical microscopy (OLYMPUS, BX60, Japan) and SEM (Gemini, Zeiss, Ultra 55, Germany) to image the morphologies of the MoS_2/SiO_2 surfaces on the Si substrates with different magnifications, respectively. We used a Raman spectrometer (alpha300 R Microscope, WITec, Germany) to evaluate the quality of the MoS_2 films on the SiO_2 surface. For the Raman scans with areas of 15 μm × 15 μm (100 × 100 points per map), we used a laser with a wavelength of 532 nm, a laser power of 1.5 mW, and an integration time of 0.3 s. For the Raman scans with the areas of 5 μm × 5 μm (25 × 25 points per map), we used a laser with a wavelength of 532 nm, a laser power of 1 mW, and an integration time of 3 s. To analyze the topography of the MoS_2/SiO_2 surfaces before and after exposing MoS_2 on the SiO_2/Si substrates to VHF for different times, we used an AFM tool (Dimension Icon, Bruker) with a cantilever (Olympus AC240TM) and an AFM tip (tip radius = 15 nm) in tapping mode.

3. RESULTS AND DISCUSSION

In our experiments, we used CVD-grown MoS_2 on a 285 nm thick SiO_2 layer on a silicon (Si) substrate, which was purchased from 2D Semiconductors Inc. (USA). The CVD-grown MoS_2 was composed of domains with continuous MoS_2 films without visible grain boundaries (Figure S1a), as well as domains in which there were presumed visible grain boundaries between the adjacent MoS_2 grains that were incompletely stitched to each other (Figure S1b). First, we evaluated and confirmed the quality of the pristine MoS_2 samples using Raman spectroscopy (Figure S2). The typical E^1_{2g} band position (385.4 cm^{-1}) and A_{1g} band position (406 cm^{-1}) depict the single-layer MoS_2 (Figure S2e). Furthermore, we used Raman spectroscopy to indicate the presence of grain boundaries between the adjacent MoS_2 grains that were incompletely stitched to each other (Figure S2b−d). In these measurements, we also found E^1_{2g} and A_{1g} bands in the Raman spectrum at the grain boundaries (Figure S2d,e), which can be attributed to the fact that the width of a MoS_2 grain boundary is smaller than the diameter of the Raman laser spot (~400 nm), as indicated in Figure S2d by the red and blue solid circles. Thus, the laser spot always overlaps either one or both sides of the adjacent MoS_2 grains when exciting the boundary region, resulting in a nonzero Raman signal of MoS_2. The surface topography of a sample of pristine MoS_2 characterized by AFM further confirms that the MoS_2 grains were incompletely stitched to each other (Figure S3).

To evaluate the proposed approach for visualizing grain boundaries in a single MoS_2 layer on a SiO_2 substrate, we exposed a sample with a large continuous MoS_2 film without visible grain boundaries (Figure 1a) to VHF at 40 °C for 120 s (see Experimental Section). After VHF exposure, line patterns became visible and distinct within the continuous film in both SEM (Figure 1b) and optical microscopy images (Figure 1c,d). The SEM (Figure 1a,b) and optical microscopy images (Figure 1c,d) were taken at the same position of the same chip. In the images, it can be seen that the areas enclosed by a line pattern are of the order of 1 μm to several μm. We tentatively assign these line patterns to the grain boundaries in the MoS_2 film.

https://dx.doi.org/10.1021/acsami.0c06910
ACS Appl. Mater. Interfaces 2020, 12, 34049−34057

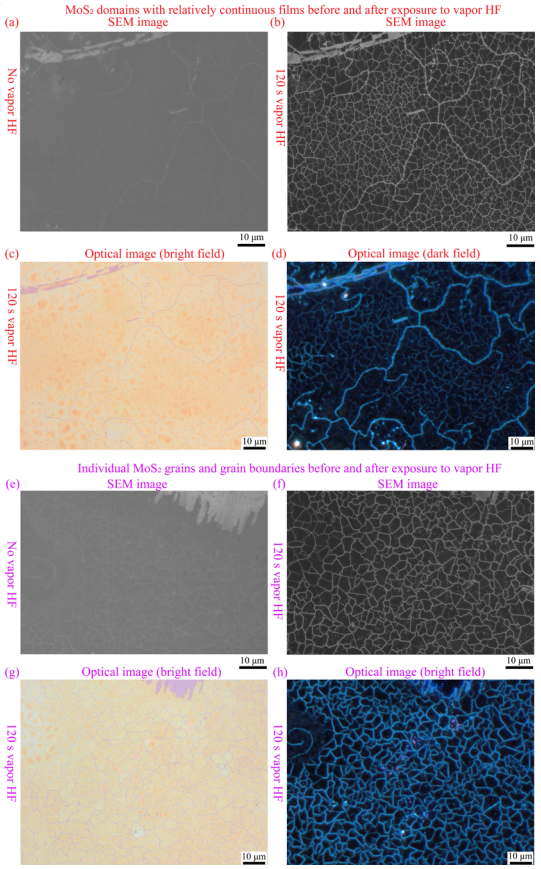

Figure 1. SEM and optical microscopy observation of the top view of a single layer of CVD-grown MoS_2 on a SiO_2 surface before and after exposure to VHF for 120 s. (a) SEM image of a continuous CVD-grown MoS_2 film on a SiO_2 substrate without visible grain boundaries or line patterns. (b) SEM image, (c) optical image, and (d) optical dark-field image of MoS_2 of the same area as (a) after exposure to VHF for 120 s. After exposure to VHF for 120 s, line patterns are visible within the continuous MoS_2 film. (e) SEM image of CVD-grown MoS_2 on a SiO_2 substrate, with visible MoS_2 grain boundaries between the adjacent grains that were not completely stitched to each other during CVD growth. (f) SEM image, (g) optical image, and (h) optical dark-field image of the same position as (e) after exposure to VHF for 120 s. After exposure to VHF for 120 s, the previously visible grain boundaries in the MoS_2 film get more pronounced, indicating that the VHF interaction and resulting line patterns occur at the MoS_2 grain boundaries.

To further explore this, we selected a chip area in which the MoS_2 film on the SiO_2 surface contained distinguishable individual grains and grain boundaries prior to VHF exposure (Figure 1e), caused by incomplete growth and stitching of the adjacent MoS_2 grains. After exposing this sample to VHF at 40 °C for 120 s, we found that the same type of line pattern in the SiO_2 layer appeared at the locations of the previously visible grain boundaries (Figure 1f–h). Also, here, the SEM and optical microscopy images in Figure 1e–h were taken from the same position of the chip. Furthermore, we investigated a chip area where a continuous MoS_2 film was located directly next to a MoS_2 film, in which grain boundaries and individual grains were visible, caused by incomplete growth and stitching of the adjacent MoS_2 grains. After exposing this sample to VHF at 40 °C for 120 s, we again observed that the same type of line pattern in the SiO_2 layer appeared at the locations of the previously visible grain boundaries, with a comparable pattern appearing in the area of the continuous film (Figure S4a,b). Interestingly, there are thinner line patterns within the large-area grain boundaries of the MoS_2 sample after exposure to VHF for 120 s, indicating that the visible larger grains are composed of several small grains (Figure S4). It should be noted that line defects other than grain boundaries, such as wrinkles in 2D materials, are easily introduced when a 2D material is transferred from its original growth substrate to a new target substrate. In contrast, the samples in our experiments consist of single-layer MoS_2 that is directly grown on the SiO_2 surface of the Si substrate by CVD, thus avoiding the transfer of the 2D material. Therefore, the MoS_2 samples used in our experiments most likely do contain only few or no wrinkles that may interfere with the visualization of the grain boundaries in MoS_2 by VHF exposure.

To explore the impact of the VHF exposure time on the resulting line patterns in both the continuous CVD-grown MoS_2 films and individual domains placed on a SiO_2 substrate, we exposed such samples to VHF at 40 °C for different times, that is, 30, 60, and 120 s. We observed that the line patterns appear increasingly pronounced with the increasing exposure time to VHF (Figures 2 and 3). We also observed that the patterns did not change in structure for the different evaluated VHF exposure times (Figures 2 and 3). Generally, when the VHF exposure time was increased from 30 to 60 and to 120 s, thin line patterns appeared inside the large MoS_2 domains and became increasingly distinct when the VHF exposure time was

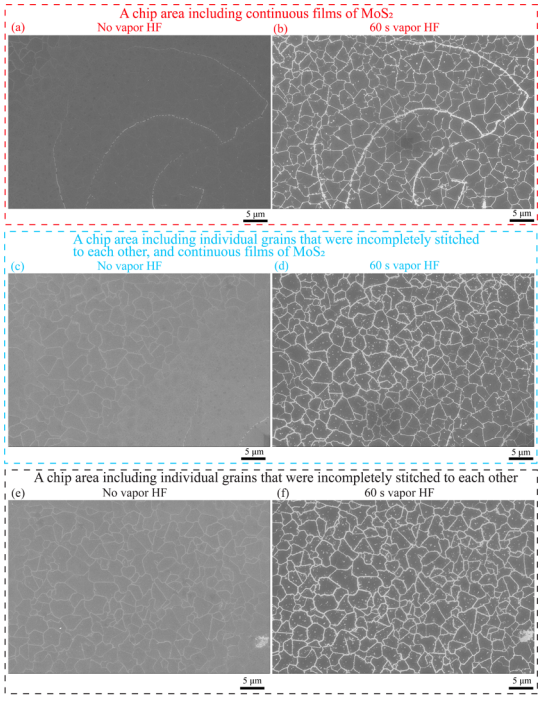

Figure 2. SEM images with the top view of CVD-grown MoS_2 on SiO_2 before and after exposure to VHF for 60 s. (a,b) SEM images of a chip area with a continuous MoS_2 film without visible grain boundaries, before (a) and after (b) exposure to VHF for 60 s. (c,d) SEM images of a chip containing both an area with a continuous MoS_2 film in which the grain boundaries are not visible and an area in which individual MoS_2 grains are visible, before (c) and after (d) exposure to VHF for 60 s. (e,f) SEM images of a sample in which the MoS_2 grains were not completely stitched to each other during CVD growth, before (e) and after (f) exposure to VHF for 60 s.

https://dx.doi.org/10.1021/acsami.0c06910
ACS Appl. Mater. Interfaces 2020, 12, 34049−34057

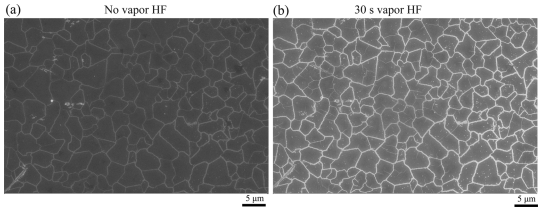

Figure 3. SEM images with the top view of CVD-grown MoS_2 on SiO_2 before and after exposure to VHF for 30 s. (a,b) SEM images of a sample in which the MoS_2 grains were not completely stitched to each other during CVD growth, before (a) and after (b) exposure to VHF for 30 s.

increased to 120 s (Figures 1−3 and S4). This indicates that a longer time (i.e., 120 s) of exposure to VHF reveals more information about the grain boundaries in MoS_2 than shorter VHF exposure time (i.e., 30 and 60 s). This is in agreement with the observation of grain boundaries in CVD-grown graphene on SiO_2/Si substrates after exposure to VHF.[43]

The mechanism for observing grain boundaries in CVD-grown graphene on SiO_2/Si substrates after exposure to VHF is based on the diffusion of VHF through the defects in the graphene lattice at the grain boundaries and the different speeds of VHF etching of SiO_2 that is close to the graphene grain boundaries and that below the graphene grains.[43] In order to verify that the mechanism for the appearance of the line patterns in the SiO_2 surface covered by the MoS_2 films is the same as described above, we used AFM to image the surface topography of our samples and characterized the evolution of the MoS_2 and SiO_2 surface topography with increasing VHF exposure times (Figure 4). Before exposing our samples to VHF, we did not observe significant topographical features in the MoS_2 film on the SiO_2 surface (Figure 4a,b). The high features appearing in white in Figure 4a might be associated with the multilayered growth or the formation of by-products occurring mainly at the grain boundaries during the synthesis of CVD-grown MoS_2, which has been reported before.[46] After exposure to VHF for 30, 60, and 120 s, the surface topography near the assumed MoS_2 grain boundaries progressively increased, with the line patterns being elevated from the other areas by about 8−10 nm (Figure 4c,d), 30−35 nm (Figure 4e,f), and 50−58 nm (Figure 4g,h), respectively. At the same time, the less pronounced lines within the initially larger domains were elevated from the other areas by about 15−20 nm after exposure to VHF for 60 s (Figure 4e,f). The three-dimensional (3D) representation of the AFM data, with the surface topography of the MoS_2 samples after exposure to VHF for 30, 60, and 120 s, further illustrate that the line pattern is elevated with respect to the areas surrounded by the line pattern (Figure 5a−d). These results conclusively confirm that the VHF exposure of a MoS_2 film on a SiO_2 surface results in differential etching of SiO_2. This can be explained by an increased etch rate of SiO_2 underneath the MoS_2 crystallites where liquid water with dissolved HF can accumulate, as compared to the SiO_2 etch rate at the MoS_2 grain boundaries where SiO_2 is directly exposed to VHF and where liquid water does not accumulate (Figure 5e). Specifically, the net reaction of etching of SiO_2 with VHF results in an excess of H_2O molecules that get trapped underneath the MoS_2 grains and accumulate in a water reservoir along with the easily water-dissolvable HF.[43] In contrast, in the areas along the grain boundaries, the excess water can evaporate through the grain boundaries, and thus SiO_2 in these areas is directly exposed to VHF, resulting in a significantly lower SiO_2 etch rate along nanoporous grain boundaries. This mechanism results in the distinct line pattern of the surface topography along the nanoporous grain boundaries in the MoS_2 films that can be visualized by SEM or optical microscopy.

To evaluate the impact of VHF exposure on the quality of the MoS_2 films on a SiO_2 substrate, we exposed MoS_2 films with presumed visible grain boundaries between the adjacent MoS_2 grains to VHF for different exposure times, that is, 30, 60, and 120 s, and thereafter performed scanning micro-Raman spectroscopy on the samples. After exposing MoS_2 to VHF for 30 s (Figure 6a), the Raman spectroscopy maps of the intensities of the E^1_{2g} and A_{1g} modes of MoS_2 are still relatively strong (Figure 6a2,a3) with clear E^1_{2g} and A_{1g} band intensities (Figure 6a4,a5). This indicates that MoS_2 is of relative high quality even after exposure to VHF for 30 s. As we increased the VHF exposure time to 60 s (Figure 6b), the Raman spectroscopy maps of the intensities of the E^1_{2g} and A_{1g} modes of MoS_2 became weaker (Figure 6b2,b3), with significantly decreased E^1_{2g} and A_{1g} bands (Figure 6b4,b5). These results indicate that MoS_2 was damaged to a larger extent during the exposure to VHF for 60 s. As expected, when we further increased the VHF exposure time to 120 s (Figure 6c), the Raman spectroscopy intensity maps of the E^1_{2g} and A_{1g} modes of MoS_2 substantially weakened (Figure 6c2,c3), with very weak E^1_{2g} and A_{1g} bands (Figure 6c4,c5). This indicates that MoS_2 was substantially damaged during the exposure to VHF for 120 s. Moreover, it can be seen from Figure 6a5−c5 that the E^1_{2g} and A_{1g} bands of MoS_2 became weaker with increasing VHF exposure times, both within the grains and at the grain boundaries. This further indicates that long VHF exposure and more etching of SiO_2 underneath the MoS_2 film degrade the quality of MoS_2. As an additional reference, we characterized samples with continuous MoS_2 films using Raman spectroscopy before and after exposing them to VHF for 30, 60, and 120 s, respectively, and we found similar results (Figures S5−S8). Our Raman spectroscopy characterization shows that the exposure to VHF of MoS_2 on a SiO_2 surface for short times (i.e., 30 s) only marginally affects MoS_2, whereas the exposure to VHF of MoS_2 placed on SiO_2 for longer times (i.e. 120 s) significantly affects MoS_2.

In a previous study, we have demonstrated that grains and grain boundaries in a CVD-grown single-layer graphene on a SiO_2/Si substrate can be visualized after exposing them to VHF.[43] In the study, we used the same processing conditions for exposing and visualizing the grains in graphene as in the experiments with MoS_2 in the present study, and thus the two approaches are comparable. One advantage of the visualization of grains in MoS_2 is that single layers of MoS_2 can be directly grown on SiO_2 surfaces by CVD, which is the required substrate material for our method. In contrast, for visualizing the grains and grain boundaries in CVD-grown graphene, graphene first has to be transferred from the original growth substrate (e.g., a copper substrate) to the SiO_2/Si substrate. A disadvantage with this is that the transfer can easily introduce additional line defects such as wrinkles, folds, and cracks as well as possible contaminations such as poly(methyl methacrylate) residues in the graphene layer,[43] which can influence the results. In addition, in our previous work, we have not been able to observe the graphene surface on exactly the same position before and after exposure to VHF for

https://dx.doi.org/10.1021/acsami.0c06910
ACS Appl. Mater. Interfaces 2020, 12, 34049−34057

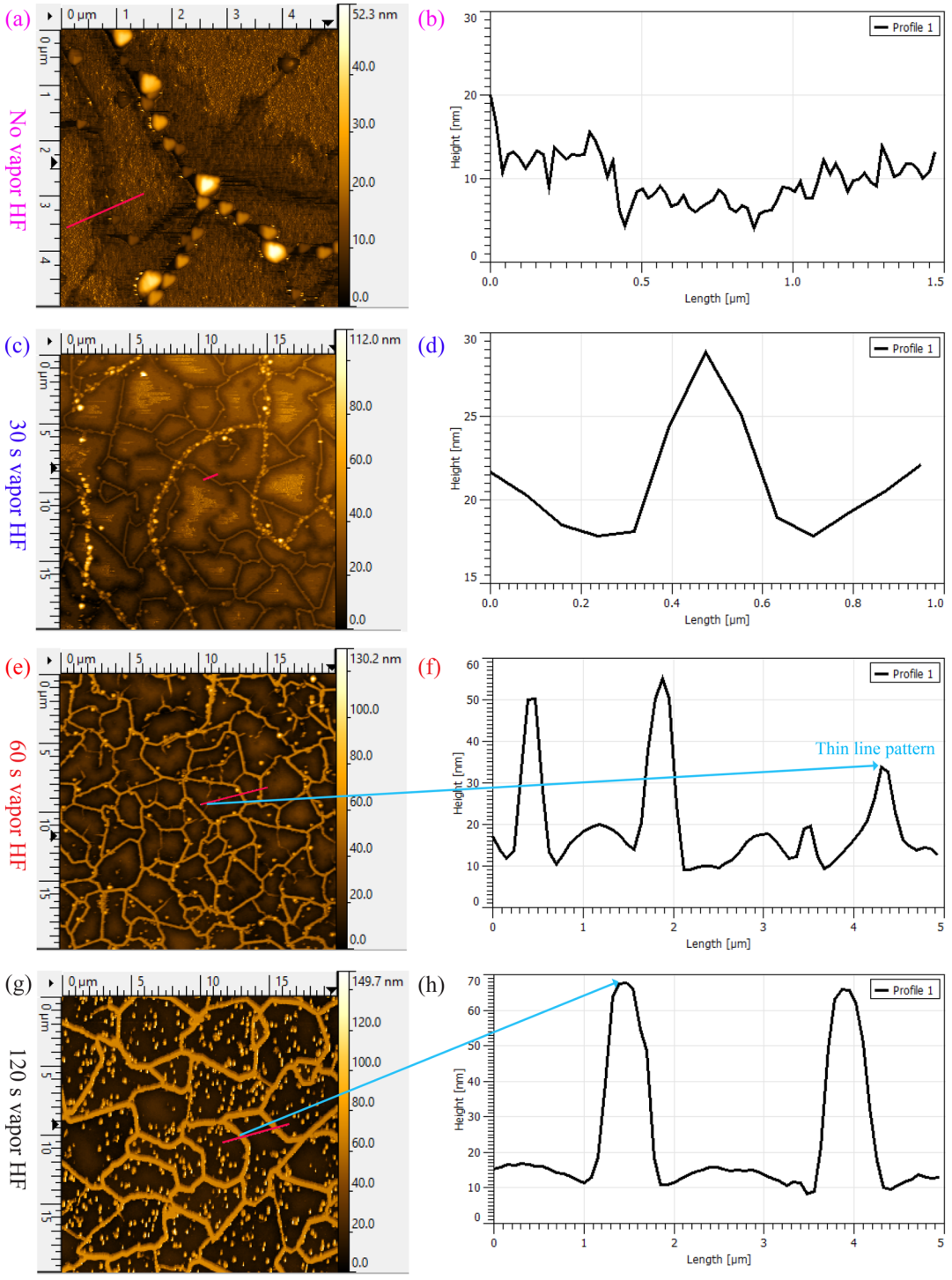

Figure 4. AFM characterization of a single layer of CVD-grown MoS_2 on a SiO_2 surface before and after exposure to VHF for 30, 60, and 120 s. (a) AFM image, with the surface topography of a MoS_2 film on a SiO_2 substrate before exposure to VHF. (b) Topographical scan of the area in (a). The corresponding data after the exposure of the sample to VHF for 30, 60, and 120 s are shown in (c,d), (e,f), and (g,h) respectively.

different times, which, to some extent, limited the accuracy of the previous results.[43] In contrast to the previous work,[43] in the present investigation, we used single-layer MoS_2 that was directly synthesized on the SiO_2/Si substrate by CVD, thereby entirely avoiding the layer transfer process with its potential disadvantages of introducing wrinkles, folds, cracks, or polymer residues. In addition, we have been able to observe MoS_2 on the SiO_2/Si substrate at exactly the same position before and after the exposure to VHF for various times, which leads to the improved accuracy of our results. We speculate that our approach may be applicable to the large-area visualization of grains and grain boundaries in single-layer 2D materials other than MoS_2 and graphene. The prerequisites for this would be that (a) the 2D material is placed on a SiO_2 surface (either grown or transferred), (b) it is a single-layer 2D material with grains larger than approximately 0.5−1 μm, and (c) the 2D material is not permeable to VHF and does not get

https://dx.doi.org/10.1021/acsami.0c06910
ACS Appl. Mater. Interfaces 2020, 12, 34049−34057

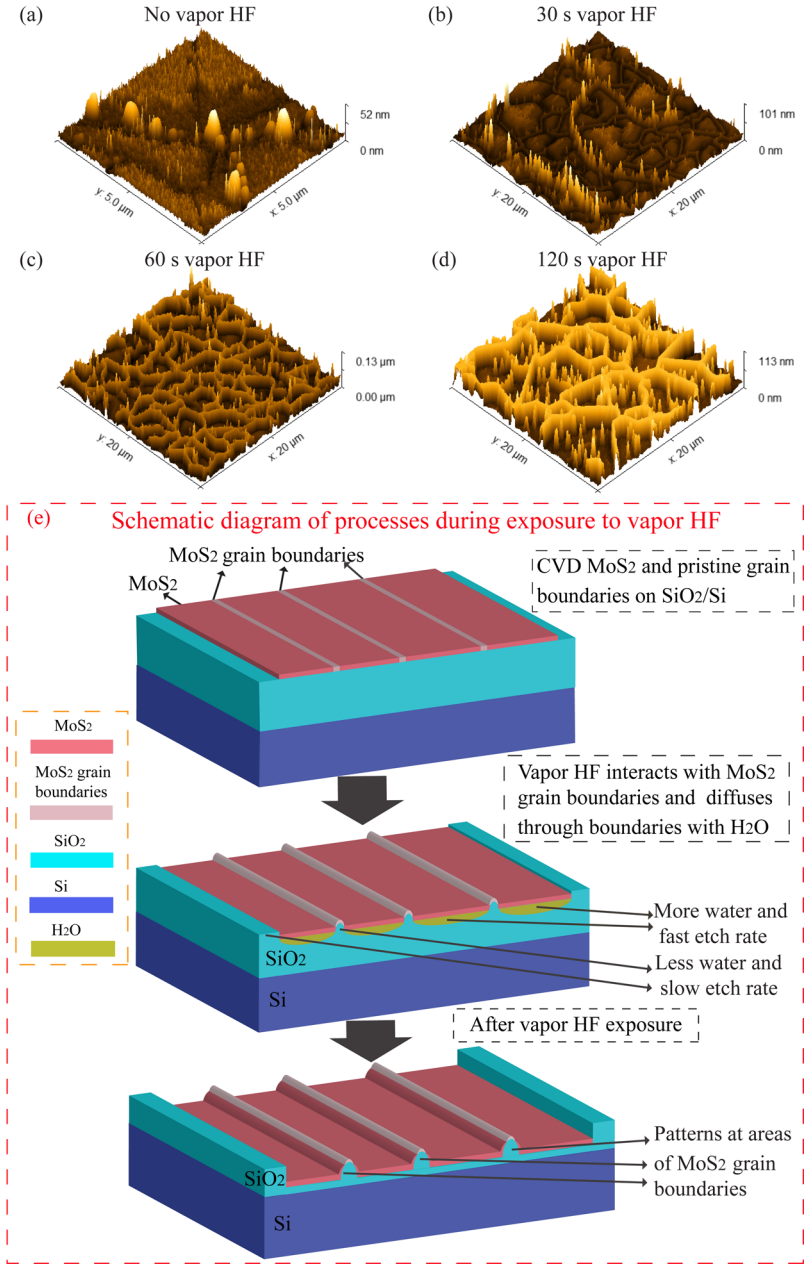

Figure 5. 3D AFM views of the surface topography of a CVD-grown single-layer MoS_2 film on a SiO_2 surface before and after exposure to VHF for 30, 60, and 120 s as well as the schematics of etching processes during the exposure to VHF. (a–d) 3D views of the surface topography of Figure 4a–d. (e) Schematics of the reaction process when MoS_2 on a SiO_2 surface is exposed to VHF.

significantly attacked by VHF during the time period of exposure (approximately 30–120 s).

In summary, we demonstrate here a simple and efficient method to visualize grain boundaries over large areas in CVD-grown MoS_2 films on a SiO_2/Si substrate. Our approach only requires VHF etching for 30–120 s and subsequent optical microscopy or SEM inspection, which are all processes and tools that are commonly available in typical cleanrooms and semiconductor labs. Although our method is invasive, that is, the sample is permanently modified in the characterization process, it has advantages such as ease of use, speed, and simple large-area analysis, which could be very useful in the development and optimization of large-scale MoS_2 synthesis processes. Our approach may also be useful for investigating and optimizing the mechanical, electrical, and chemical properties of CVD-grown MoS_2, which are strongly influenced by grain boundaries and grain sizes, thereby ultimately promoting the utilization of MoS_2 in research and its application in future 2D material devices.

4. CONCLUSIONS

We demonstrated that VHF can be used to rapidly visualize the location of grains and grain boundaries over large areas in CVD-grown single-layer MoS_2 on a SiO_2 surface by using optical microscopy, SEM imaging, or Raman spectroscopy. Our approach is based on the difference in the etching behavior of SiO_2 near the MoS_2 grain boundaries and of SiO_2 below the MoS_2 grains when exposed to VHF. The resulting microscale line patterns in the SiO_2 surface are caused by higher etch rates of SiO_2 in the areas underneath the MoS_2

https://dx.doi.org/10.1021/acsami.0c06910
ACS Appl. Mater. Interfaces 2020, 12, 34049–34057

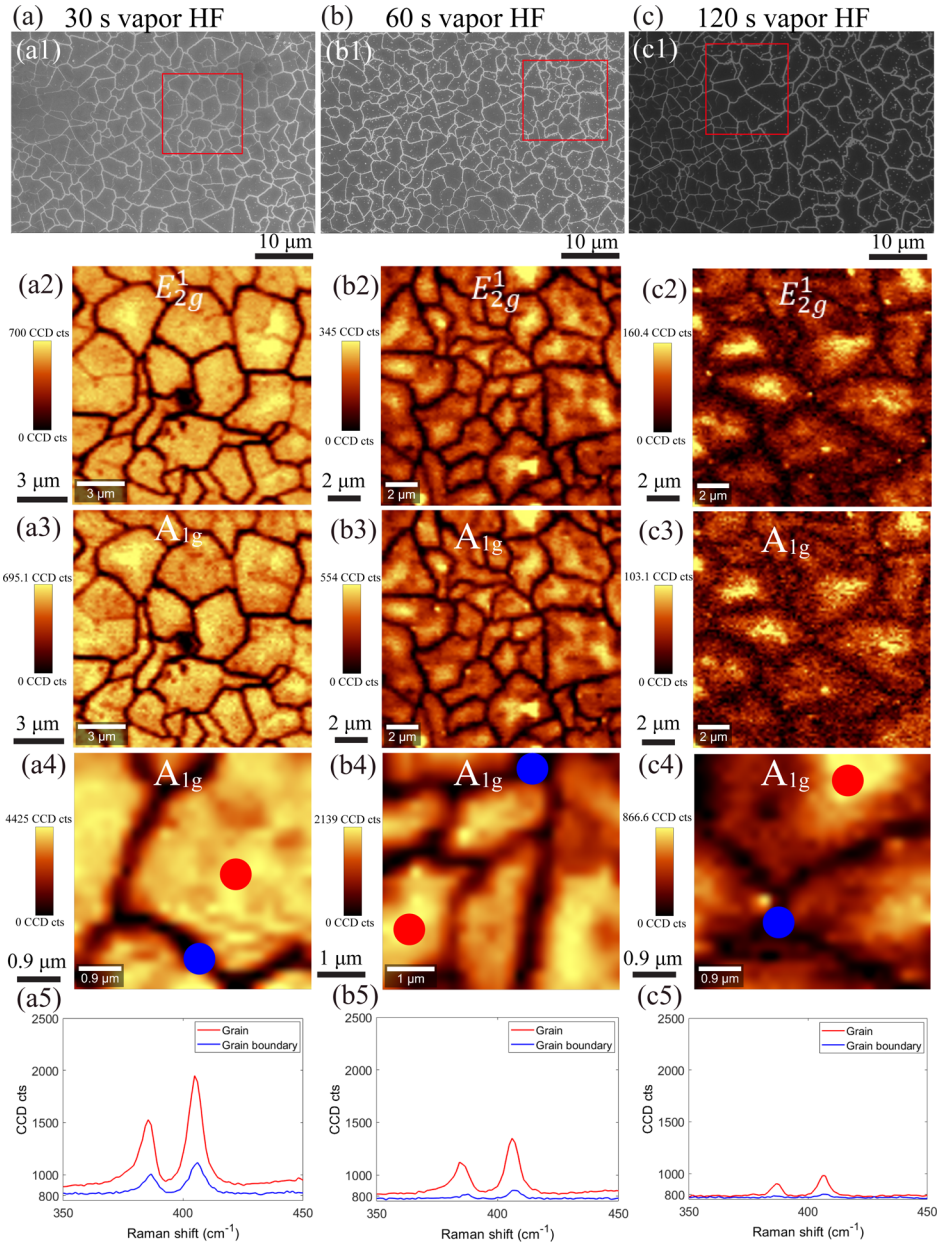

Figure 6. Raman characterization of CVD-grown MoS_2 on a SiO_2 surface after exposing it to VHF for 30, 60, and 120 s. Raman spectroscopy map of CVD-grown MoS_2 on a SiO_2 surface on a Si substrate and Raman spectroscopy map of the corresponding Si substrate after exposure to VHF for 30 s (a): maps of the intensities of the E^1_{2g} (a2) and A_{1g} modes (a3) of MoS_2 in the area of the sample that is marked by the red box in the optical image (a1). (a4) Close-up of (a3). (a5) Raman spectra of the two areas that are marked in (a4) by red and blue solid circles. (b,c) Corresponding data of MoS_2 on a SiO_2 surface after exposure to VHF for 60 s (b) and 120 s (c).

grains, thereby causing topographical differences between the areas where grains and grain boundary-based lattice defects in the MoS_2 film are located. The higher etch rate of SiO_2 in the areas underneath the MoS_2 grains is ascribed to the accumulation of liquid H_2O with dissolved HF underneath the MoS_2 grains. By contrast, there is no trapped liquid H_2O in the areas of SiO_2 near the grain boundaries. Our approach will be useful for efficient and large-scale imaging of the MoS_2 grains and grain boundaries, with utility in the development, optimization, and monitoring of the MoS_2 growth by CVD and in the evaluation of MoS_2 devices.

■ ASSOCIATED CONTENT

Supporting Information

The Supporting Information is available free of charge at https://pubs.acs.org/doi/10.1021/acsami.0c06910.

SEM and Raman characterizations (PDF)

■ AUTHOR INFORMATION

Corresponding Authors

Xuge Fan − *Division of Micro and Nanosystems, School of Electrical Engineering and Computer Science, KTH Royal Institute of Technology, SE-10044 Stockholm, Sweden;* orcid.org/0000-0002-8811-1615; Email: xuge@eecs.kth.se

https://dx.doi.org/10.1021/acsami.0c06910
ACS Appl. Mater. Interfaces 2020, 12, 34049−34057

Georg S. Duesberg − *Faculty of Electrical Engineering and Information Technology, EIT2 Universität der Bundeswehr München, 85577 Neubiberg, Germany*; Email: duesberg@unibw.de

Frank Niklaus − *Division of Micro and Nanosystems, School of Electrical Engineering and Computer Science, KTH Royal Institute of Technology, SE-10044 Stockholm, Sweden*; Email: frank.niklaus@eecs.kth.se

Authors

Rita Siris − *Faculty of Electrical Engineering and Information Technology, EIT2 Universität der Bundeswehr München, 85577 Neubiberg, Germany*

Oliver Hartwig − *Faculty of Electrical Engineering and Information Technology, EIT2 Universität der Bundeswehr München, 85577 Neubiberg, Germany*

Complete contact information is available at: https://pubs.acs.org/10.1021/acsami.0c06910

Author Contributions

X.F. and F.N. conceived and designed the experiments. X.F. performed the experiments and optical, SEM, and AFM characterizations and wrote the manuscript. R.S., O.H., and G.S.D. performed the Raman spectroscopy characterization. F.N. and G.S.D. provided the guidance in manuscript writing. All authors analyzed and discussed with the results and commented on the manuscript.

Notes

The authors declare no competing financial interest.

■ ACKNOWLEDGMENTS

We acknowledge support through the scholarship from China Scholarship Council, the Swedish Research Council (GEMS, 2015-05112), the ERC Starting Grants M&M's (277879). This project has received funding from the European Union's Horizon 2020 research and innovation program under grant agreement no. 829035 (Queformal) and no. 785219 (Graphene Flagship). Further, the authors thank the BMBF for support through the ACDC project.

■ REFERENCES

(1) Choi, W.; Choudhary, N.; Han, G. H.; Park, J.; Akinwande, D.; Lee, Y. H. Recent Development of Two-Dimensional Transition Metal Dichalcogenides and Their Applications. *Mater. Today* **2017**, *20*, 116−130.

(2) Ferrari, A. C.; Bonaccorso, F.; Fal'ko, V.; Novoselov, K. S.; Roche, S.; Bøggild, P.; Borini, S.; Koppens, F. H. L.; Palermo, V.; Pugno, N.; Garrido, J. A.; Sordan, R.; Bianco, A.; Ballerini, L.; Prato, M.; Lidorikis, E.; Kivioja, J.; Marinelli, C.; Ryhänen, T.; Morpurgo, A.; Coleman, J. N.; Nicolosi, V.; Colombo, L.; Fert, A.; Garcia-Hernandez, M.; Bachtold, A.; Schneider, G. F.; Guinea, F.; Dekker, C.; Barbone, M.; Sun, Z.; Galiotis, C.; Grigorenko, A. N.; Konstantatos, G.; Kis, A.; Katsnelson, M.; Vandersypen, L.; Loiseau, A.; Morandi, V.; Neumaier, D.; Treossi, E.; Pellegrini, V.; Polini, M.; Tredicucci, A.; Williams, G. M.; Hong, B. H.; Ahn, J.-H.; Kim, J. M.; Zirath, H.; van Wees, B. J.; van der Zant, H.; Occhipinti, L.; Matteo, A. D.; Kinloch, I. A.; Seyller, T.; Quesnel, E.; Feng, X.; Teo, K.; Rupesinghe, N.; Hakonen, P.; Neil, S. R. T.; Tannock, Q.; Löfwander, T.; Kinaret, J. Science and Technology Roadmap for Graphene, Related Two-Dimensional Crystals, and Hybrid Systems. *Nanoscale* **2015**, *7*, 4598−4810.

(3) Wang, H.; Li, C.; Fang, P.; Zhang, Z.; Zhang, J. Z. Synthesis, Properties, and Optoelectronic Applications of Two-Dimensional MoS2 and MoS2-Based Heterostructures. *Chem. Soc. Rev.* **2018**, *47*, 6101−6127.

(4) Radisavljevic, B.; Radenovic, A.; Brivio, J.; Giacometti, V.; Kis, A. Single-Layer MoS 2 Transistors. *Nat. Nanotechnol.* **2011**, *6*, 147−150.

(5) Splendiani, A.; Sun, L.; Zhang, Y.; Li, T.; Kim, J.; Chim, C.-Y.; Galli, G.; Wang, F. Emerging Photoluminescence in Monolayer MoS2. *Nano Lett.* **2010**, *10*, 1271−1275.

(6) Lopez-Sanchez, O.; Lembke, D.; Kayci, M.; Radenovic, A.; Kis, A. Ultrasensitive Photodetectors Based on Monolayer MoS_2. *Nat. Nanotechnol.* **2013**, *8*, 497−501.

(7) Sun, Z.; Martinez, A.; Wang, F. Optical Modulators with 2D Layered Materials. *Nat. Photonics* **2016**, *10*, 227−238.

(8) Yu, F.; Liu, Q.; Gan, X.; Hu, M.; Zhang, T.; Li, C.; Kang, F.; Terrones, M.; Lv, R. Ultrasensitive Pressure Detection of Few-Layer MoS2. *Adv. Mater.* **2017**, *29*, 1603266.

(9) Lee, J.; Wang, Z.; He, K.; Shan, J.; Feng, P. X.-L. High Frequency MoS2 Nanomechanical Resonators. *ACS Nano* **2013**, *7*, 6086−6091.

(10) Kalantar-zadeh, K.; Ou, J. Z. Biosensors Based on Two-Dimensional MoS2. *ACS Sens.* **2016**, *1*, 5−16.

(11) Yang, W.; Gan, L.; Li, H.; Zhai, T. Two-Dimensional Layered Nanomaterials for Gas-Sensing Applications. *Inorg. Chem. Front.* **2016**, *3*, 433−451.

(12) Li, Z.; Meng, X.; Zhang, Z. Recent Development on MoS2-Based Photocatalysis: A Review. *J. Photochem. Photobiol., C* **2018**, *35*, 39−55.

(13) Zhang, G.; Liu, H.; Qu, J.; Li, J. Two-Dimensional Layered MoS2: Rational Design, Properties and Electrochemical Applications. *Energy Environ. Sci.* **2016**, *9*, 1190−1209.

(14) Lee, Y.-H.; Zhang, X.-Q.; Zhang, W.; Chang, M.-T.; Lin, C.-T.; Chang, K.-D.; Yu, Y.-C.; Wang, J. T.-W.; Chang, C.-S.; Li, L.-J.; Lin, T.-W. Synthesis of Large-Area MoS2 Atomic Layers with Chemical Vapor Deposition. *Adv. Mater.* **2012**, *24*, 2320−2325.

(15) Zhan, Y.; Liu, Z.; Najmaei, S.; Ajayan, P. M.; Lou, J. Large-Area Vapor-Phase Growth and Characterization of MoS2 Atomic Layers on a SiO2 Substrate. *Small* **2012**, *8*, 966−971.

(16) Qian, S.; Yang, R.; Lan, F.; Xu, Y.; Sun, K.; Zhang, S.; Zhang, Y.; Dong, Z. Growth of Continuous MoS2 Film with Large Grain Size by Chemical Vapor Deposition. *Mater. Sci. Semicond. Process.* **2019**, *93*, 317−323.

(17) Kwak, T.; Lee, J.; So, B.; Choi, U.; Nam, O. Growth Behavior of Wafer-Scale Two-Dimensional MoS2 Layer Growth Using Metal-Organic Chemical Vapor Deposition. *J. Cryst. Growth* **2019**, *510*, 50−55.

(18) van der Zande, A. M.; Huang, P. Y.; Chenet, D. A.; Berkelbach, T. C.; You, Y.; Lee, G.-H.; Heinz, T. F.; Reichman, D. R.; Muller, D. A.; Hone, J. C. Grains and Grain Boundaries in Highly Crystalline Monolayer Molybdenum Disulphide. *Nat. Mater.* **2013**, *12*, 554−561.

(19) Najmaei, S.; Liu, Z.; Zhou, W.; Zou, X.; Shi, G.; Lei, S.; Yakobson, B. I.; Idrobo, J.-C.; Ajayan, P. M.; Lou, J. Vapour Phase Growth and Grain Boundary Structure of Molybdenum Disulphide Atomic Layers. *Nat. Mater.* **2013**, *12*, 754−759.

(20) Ji, Q.; Kan, M.; Zhang, Y.; Guo, Y.; Ma, D.; Shi, J.; Sun, Q.; Chen, Q.; Zhang, Y.; Liu, Z. Unravelling Orientation Distribution and Merging Behavior of Monolayer MoS2 Domains on Sapphire. *Nano Lett.* **2015**, *15*, 198−205.

(21) Zhou, W.; Zou, X.; Najmaei, S.; Liu, Z.; Shi, Y.; Kong, J.; Lou, J.; Ajayan, P. M.; Yakobson, B. I.; Idrobo, J.-C. Intrinsic Structural Defects in Monolayer Molybdenum Disulfide. *Nano Lett.* **2013**, *13*, 2615−2622.

(22) Yazyev, O. V.; Louie, S. G. Electronic Transport in Polycrystalline Graphene. *Nat. Mater.* **2010**, *9*, 806−809.

(23) Ghorbani-Asl, M.; Enyashin, A. N.; Kuc, A.; Seifert, G.; Heine, T. Defect-Induced Conductivity Anisotropy in MoS${}_{2}$ Monolayers. *Phys. Rev. B: Condens. Matter Mater. Phys.* **2013**, *88*, 245440.

(24) Hus, S. M.; Li, A.-P. Spatially-Resolved Studies on the Role of Defects and Boundaries in Electronic Behavior of 2D Materials. *Prog. Surf. Sci.* **2017**, *92*, 176−201.

(25) Bernardi, M.; Palummo, M.; Grossman, J. C. Extraordinary Sunlight Absorption and One Nanometer Thick Photovoltaics Using

Two-Dimensional Monolayer Materials. *Nano Lett.* **2013**, *13*, 3664−3670.
(26) Ganatra, R.; Zhang, Q. Few-Layer MoS2: A Promising Layered Semiconductor. *ACS Nano* **2014**, *8*, 4074−4099.
(27) Dang, K. Q.; Spearot, D. E. Effect of Point and Grain Boundary Defects on the Mechanical Behavior of Monolayer MoS2 under Tension via Atomistic Simulations. *J. Appl. Phys.* **2014**, *116*, 013508.
(28) Liu, K.; Wu, J. Mechanical Properties of Two-Dimensional Materials and Heterostructures. *J. Mater. Res.* **2016**, *31*, 832−844.
(29) Shi, Y.; Huang, J.-K.; Jin, L.; Hsu, Y.-T.; Yu, S. F.; Li, L.-J.; Yang, H. Y. Selective Decoration of Au Nanoparticles on Monolayer MoS_2 Single Crystals. *Sci. Rep.* **2013**, *3*, 1839.
(30) Lin, Z.; Carvalho, B. R.; Kahn, E.; Lv, R.; Rao, R.; Terrones, H.; Pimenta, M. A.; Terrones, M. Defect Engineering of Two-Dimensional Transition Metal Dichalcogenides. *2D Mater.* **2016**, *3*, 022002.
(31) Hu, Z.; Wu, Z.; Han, C.; He, J.; Ni, Z.; Chen, W. Two-Dimensional Transition Metal Dichalcogenides: Interface and Defect Engineering. *Chem. Soc. Rev.* **2018**, *47*, 3100−3128.
(32) Huang, Y. L.; Chen, Y.; Zhang, W.; Quek, S. Y.; Chen, C.-H.; Li, L.-J.; Hsu, W.-T.; Chang, W.-H.; Zheng, Y. J.; Chen, W.; Wee, A. T. S. Bandgap Tunability at Single-Layer Molybdenum Disulphide Grain Boundaries. *Nat. Commun.* **2015**, *6*, 6298.
(33) Vancsó, P.; Magda, G. Z.; Pető, J.; Noh, J.-Y.; Kim, Y.-S.; Hwang, C.; Biró, L. P.; Tapasztó, L. The Intrinsic Defect Structure of Exfoliated MoS_2 Single Layers Revealed by Scanning Tunneling Microscopy. *Sci. Rep.* **2016**, *6*, 29726.
(34) Prado, M. C.; Nascimento, R.; Faria, B. E. N.; Matos, M. J. S.; Chacham, H.; Neves, B. R. A. Nanometre-Scale Identification of Grain Boundaries in MoS2through Molecular Decoration. *Nanotechnology* **2015**, *26*, 475702.
(35) Yin, X.; Ye, Z.; Chenet, D. A.; Ye, Y.; O'Brien, K.; Hone, J. C.; Zhang, X. Edge Nonlinear Optics on a MoS_2; Atomic Monolayer. *Science* **2014**, *344*, 488−490.
(36) Hsu, W.-T.; Zhao, Z.-A.; Li, L.-J.; Chen, C.-H.; Chiu, M.-H.; Chang, P.-S.; Chou, Y.-C.; Chang, W.-H. Second Harmonic Generation from Artificially Stacked Transition Metal Dichalcogenide Twisted Bilayers. *ACS Nano* **2014**, *8*, 2951−2958.
(37) Park, S.; Kim, M. S.; Kim, H.; Lee, J.; Han, G. H.; Jung, J.; Kim, J. Spectroscopic Visualization of Grain Boundaries of Monolayer Molybdenum Disulfide by Stacking Bilayers. *ACS Nano* **2015**, *9*, 11042−11048.
(38) Li, Y.; Rao, Y.; Mak, K. F.; You, Y.; Wang, S.; Dean, C. R.; Heinz, T. F. Probing Symmetry Properties of Few-Layer MoS2 and h-BN by Optical Second-Harmonic Generation. *Nano Lett.* **2013**, *13*, 3329−3333.
(39) Karvonen, L.; Säynätjoki, A.; Huttunen, M. J.; Autere, A.; Amirsolaimani, B.; Li, S.; Norwood, R. A.; Peyghambarian, N.; Lipsanen, H.; Eda, G.; Kieu, K.; Sun, Z. Rapid Visualization of Grain Boundaries in Monolayer MoS 2 by Multiphoton Microscopy. *Nat. Commun.* **2017**, *8*, 15714.
(40) Ly, T. H.; Chiu, M.-H.; Li, M.-Y.; Zhao, J.; Perello, D. J.; Cichocka, M. O.; Oh, H. M.; Chae, S. H.; Jeong, H. Y.; Yao, F.; Li, L.-J.; Lee, Y. H. Observing Grain Boundaries in CVD-Grown Monolayer Transition Metal Dichalcogenides. *ACS Nano* **2014**, *8*, 11401−11408.
(41) Kim, D. W.; Ok, J. M.; Jung, W.-B.; Kim, J.-S.; Kim, S. J.; Choi, H. O.; Kim, Y. H.; Jung, H.-T. Direct Observation of Molybdenum Disulfide, MoS2, Domains by Using a Liquid Crystalline Texture Method. *Nano Lett.* **2015**, *15*, 229−234.
(42) Sun, L.; Zheng, J. Optical Visualization of MoS2 Grain Boundaries by Gold Deposition. *Sci. China Mater.* **2018**, *61*, 1154−1158.
(43) Fan, X.; Wagner, S.; Schädlich, P.; Speck, F.; Kataria, S.; Haraldsson, T.; Seyller, T.; Lemme, M. C.; Niklaus, F. Direct Observation of Grain Boundaries in Graphene through Vapor Hydrofluoric Acid (VHF) Exposure. *Sci. Adv.* **2018**, *4*, No. eaar5170.
(44) Witvrouw, A.; Bois, B. D.; Moor, P. D.; Verbist, A.; Hoof, C. A. V.; Bender, H.; Baert, C. Comparison between Wet HF Etching and Vapor HF Etching for Sacrificial Oxide Removal. *Micromachining and Microfabrication Process Technology VI*; International Society for Optics and Photonics, 2000; Vol. *4174*, pp 130−141.
(45) Helms, C. R.; Deal, B. E. Mechanisms of the HF/H2O Vapor Phase Etching of SiO2. *J. Vac. Sci. Technol., A* **1992**, *10*, 806−811.
(46) O'Brien, M.; McEvoy, N.; Hallam, T.; Kim, H.-Y.; Berner, N. C.; Hanlon, D.; Lee, K.; Coleman, J. N.; Duesberg, G. S. Transition Metal Dichalcogenide Growth via Close Proximity Precursor Supply. *Sci. Rep.* **2015**, *4*, 7374.

https://dx.doi.org/10.1021/acsami.0c06910
ACS Appl. Mater. Interfaces 2020, 12, 34049−34057